Kondo conductance across the smallest spin 1/2 radical molecule

note finali coverpage

(Article begins on next page)

16 January 2024

Kondo conductance across the smallest spin 1/2 radical molecule

Ryan Requist,[1] Silvio Modesti,[2] Pier Paolo Baruselli,[1, 3, 4]
Alexander Smogunov,[5] Michele Fabrizio,[1, 4] and Erio Tosatti[1, 4, 6]

[1] SISSA, Via Bonomea 265, Trieste 34136, Italy
[2] Physics Department, University of Trieste, Via Valerio 2, Trieste 34127, Italy
[3] Institute for Theoretical Physics, TU Dresden, 01069 Dresden, Germany
[4] CNR-IOM Democritos, Via Bonomea 265, Trieste 34136, Italy
[5] CEA, IRAMIS, SPCSI, F-91191 Gif-sur-Yvette Cedex, France
[6] ICTP, Strada Costiera 11, Trieste 34151, Italy

Molecular contacts are generally poorly conducting because their energy levels tend to lie far from the Fermi energy of the metal contact, necessitating undesirably large gate and bias voltages in molecular electronics applications. Molecular radicals are an exception because their partly filled orbitals undergo Kondo screening, opening the way to electron passage even at zero bias. While that phenomenon has been experimentally demonstrated for several complex organic radicals, quantitative theoretical predictions have not been attempted so far. It is therefore an open question whether and to what extent an ab initio-based theory is able to make accurate predictions for Kondo temperatures and conductance lineshapes. Choosing nitric oxide NO as a simple and exemplary spin 1/2 molecular radical, we present calculations based on a combination of density functional theory and numerical renormalization group (DFT+NRG) predicting a zero bias spectral anomaly with a Kondo temperature of 15 K for NO/Au(111). A scanning tunneling spectroscopy study is subsequently carried out to verify the prediction, and a striking zero bias Kondo anomaly is confirmed, still quite visible at liquid nitrogen temperatures. Comparison shows that the experimental Kondo temperature of about 43 K is larger than the theoretical one, while the inverted Fano lineshape implies a strong source of interference not included in the model. These discrepancies are not a surprise, providing in fact an instructive measure of the approximations used in the modeling, which supports and qualifies the viability of the DFT+NRG approach to the prediction of conductance anomalies in larger molecular radicals.

Keywords: nanocontacts, Anderson impurity model, ballistic conductance, phase shift

Electron transport through molecules adsorbed on metallic surfaces or suspended between metal leads is the basic ingredient of molecular electronics [1–3]. Because the highest occupied and lowest unoccupied molecular orbitals rarely lie close to the Fermi energy, electrons must generally tunnel through the molecule, making the zero bias conductance much smaller than $G_0 = 2e^2/h$, the conductance quantum, whenever gating is not easily achieved, as is the case in mechanical break junctions and STM. That problem does not persist for molecular *radicals*, where one or more molecular orbitals are singly occupied, generally resulting in a net spin. When brought into contact with a metal, the radical's spin is Kondo screened [4], leading to a zero bias conductance which may be of order G_0 with a Fano-like anomaly below the Kondo temperature T_K [5, 6] and no need for gating. One reason for practical interest in such anomalies is the sensitivity of the conductance to external control parameters such as magnetic fields and mechanical strain [7]. Several molecular contacts have been studied [8], involving both adsorbed [9–16] and contact-bridging [7, 17–19] molecules. None so far involved a radical molecule that is both simple and spin 1/2, and the Kondo anomalies were not predicted from first principles, ahead of experiment. Both the intrinsic complexity of the contact between a large molecular radical and a metal, and the unavailability of quantitatively tested *ab initio* electronic structure based approaches to Kondo conductance have so far re-

stricted the theoretical work to the role of *a posteriori* support of STM and break junction zero bias anomaly data. It is therefore important to achieve a first principles predictive capability of Kondo conductance anomalies across molecular radicals and ascertain its reliability. To that end, we put to work a DFT+NRG method devised and implemented earlier in our group [20–22] but not yet verified by experiment. While other strategies with similar goals have also been proposed in Refs. [23–26], we can now demonstrate the predictive power as well as the limitations of our procedure in a specific test case where direct comparison with experiment is possible.

Seeking a molecular radical Kondo system of the utmost simplicity and stimulated by the experimentally observed Kondo screening of the $S = 1$ radical O_2 [12], we singled out nitric oxide, NO, as the smallest and simplest $S = 1/2$ radical molecule which might display a Kondo conductance anomaly in an adsorbed state. We have therefore applied our theoretical program to STM conductance of the NO radical adsorbed on the Au(111) surface. NO is an interesting test case, in the past only qualitatively considered as a prototype of radical-surface Kondo interactions [27, 28], while recently it has been used instead to quench the spin state of larger molecular radicals such as porphyrins and phthalocyanines [29].

Starting with DFT calculations of an idealized Au(111)/ NO/STM tip geometry as shown in Fig. 1, we determined the adsorption geometry and the persis-
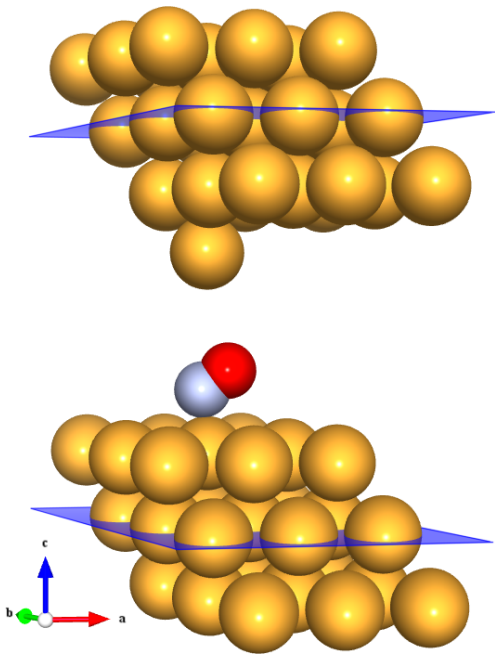
FIG. 1: Model STM geometry for NO/Au(111). The scattering region shown contains one NO molecule and 28 Au atoms; it satisfies periodic boundary conditions in the transverse direction and is bounded by two planes in the c direction, where the potential is smoothly matched to the potential of bulk gold. NO is shown in the optimal on-top adsorption geometry, where the molecule is bent by about 60 degrees. Figure produced using VESTA [46].
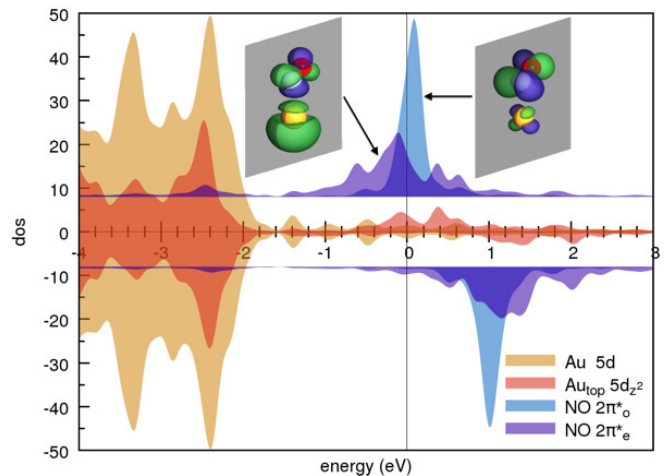

FIG. 2: Projected density of states for NO/Au(111). Spin up states are plotted as positive values, spin down as negative. The density of states of the NO $2\pi^*$ molecular orbitals (insets) are estimated from weighted sums of the projections on N and O p orbitals. The Fermi energy is indicated by a vertical line. The $2\pi^*$ states of NO and the d_{z^2} states of the top-site Au atom, $\mathrm{Au_{top}}$, are shifted and scaled for visibility.

tence of a nonzero spin state carried by the $2\pi^*$ orbitals of NO. A two-orbital Anderson model describing their hybridization with the gold surface Fermi sea was constructed and its parameters adjusted to quantitatively reproduce the DFT results. The NRG solution of the Anderson model (*NRG Results*) determined which of the two $2\pi^*$ orbitals, namely the one with odd symmetry, is eventually screened at the Kondo fixed point. A spectral function peak and a zero bias conductance anomaly were predicted with a Kondo temperature of about 15 K (half width at half maximum (HWHM) of 5 meV) [47]. To check these predictions we carried out STM/STS experiments (*STM/STS Results*) for NO/Au(111). A clear Kondo anomaly was found with an experimental Kondo temperature of about 43 K (HWHM=16 meV). The observed conductance lineshape near zero bias, a sharp dip, is also quite close but exactly complementary to the calculated Kondo spectral peak. The broad agreement with experiment and especially the discrepancies represent an important critical validation, pointing out physical variables to be included in future calculations.

First Principles Calculations and Modeling

The initial step is a DFT calculation (*Materials and Methods* and *SI Text*) of NO adsorbed on an unreconstructed Au(111) surface, adopted here as an approximation to the face-centered cubic (fcc) domains of the

"herringbone" reconstructed Au(111) surface [30]. Our calculations show that the only stable NO adsorption geometry is on-top, with N pointing down toward a Au surface atom and, remarkably, a tilt angle of nearly 60 degrees as illustrated in Fig. 1. NO also binds (with lower binding energy) at Au(111) bridge and hollow sites. However, in the low coverage limit these adsorption states are only stable when NO is constrained to be upright, for otherwise there is no barrier against migration to the optimal tilted on-top adsorption state. The calculated on-top adsorption energy 320 meV is weak and compares well with an estimated 400 meV from temperature programmed desorption spectroscopy [4].

Consistent with that weak adsorption state, spin-polarized DFT shows the persistence of a magnetic moment close to one Bohr magneton, meaning that adsorbed NO retains its radical character as in vacuum. Both $2\pi^*$ molecular orbital resonances, their degeneracy lifted in the tilted on-top adsorption state, cross the gold Fermi level (Fig. S1). This is an important point – the DFT calculation partitions the single unpaired electron approximately equally between the two $2\pi^*$ orbitals, despite a significant splitting of the orbital energy levels due to the large tilt angle. Although the evidence of NO tilting in our STM images is not firmly established, its occurrence is convincingly stabilized by the resulting hybridization with the Au surface. Of the total impurity magnetization ~55% originates from the more hybridized even $2\pi^*$ orbital with lobes in the $\mathrm{Au_{top}}$-N-O plane (see inset of Fig. S1), and the remaining 45% from the less hybridized odd $2\pi^*$ orbital normal to that plane.

To calculate the hybridization of the molecular orbitals with the gold surface, we use the information contained

in the calculated phase shifts of gold conduction electrons scattering off the adsorbed molecule [20–22]. The quantum mechanical scattering problem is solved numerically for the geometry in Fig. 1 using pwcond [32] (*Materials and Methods*), which provides spin resolved phase shifts for the relevant symmetry channels. Here we focus on two symmetries, namely even (e) and odd (o) under reflection across the Au_{top}-N-O plane, corresponding to the strongly and weakly hybridized NO $2\pi^*$ orbitals, respectively. It should be noted for later discussion that the scattering problem involved only the Bloch states of bulk Au and not those of the surface states.

The next step of our theoretical protocol is to define an Anderson model Hamiltonian including channels of both symmetries

$$H = \epsilon_e n_e + \epsilon_o n_o + \sum_{\alpha=e,o} \sum_k (V_{k\alpha} c_k^\dagger c_\alpha + V_{k\alpha}^* c_\alpha^\dagger c_k) + H_{int}, \quad (1)$$

where the subscript $\alpha = e/o$ stands for the $2\pi^*_{e/o}$ state, $V_{k\alpha}$ describes hybridization with gold conduction states, and H_{int} contains all of the interactions in the $2\pi^*$ manifold. When the molecule is brought down to the surface in an upright configuration at the on-top, fcc or hexagonal close-packed (hcp) sites, the crystal field lowers the cylindrical symmetry of the isolated molecule to C_{3v}. Further tilting of the molecule at the on-top site breaks C_{3v} symmetry and lifts the $2\pi^*$ degeneracy. The splitting of the $2\pi^*_e$ and $2\pi^*_o$ levels and their unequal hybridization with gold conduction states, at first sight an irrelevant detail, is actually crucial to the Kondo physics, as we shall discuss below.

The molecular orbitals hybridize with both surface and bulk states. Surface state hybridization affects the electronic structure of adsorption but only weakly. This is borne out in our slab calculations, where the adsorption energy converges already for 5 layers, while the energies of the surface states of the top and bottom of the slab—strongly split by their mutual interaction—do not converge until ∼23 layers [33]. If surface state hybridization had a significant effect on the electronic structure, one would expect the adsorption energy to converge more slowly than it does. Surface states decay exponentially inside the bulk, and therefore their contribution to the hybridization and phase shifts, and hence to the conductance anomalies, are invisible in our scattering calculations, which involve only bulk scattering channels. We checked that the *ab initio* estimates of the molecular orbital hybridization linewidths $2\Gamma_\alpha = 2\pi \sum_k |V_{k\alpha}|^2 \delta(\epsilon_k - \epsilon_F)$ are well converged with respect to the number of layers of the slab.

The interaction Hamiltonian is now written in terms of the $2\pi^*$ states as

$$H_{int} = U_e n_{e\uparrow} n_{e\downarrow} + U_o n_{o\uparrow} n_{o\downarrow} + U_{eo} n_e n_o + J_H \mathbf{S}_e \cdot \mathbf{S}_o + W, \quad (2)$$

where the U terms are intra-channel and inter-channel Hubbard interactions, the J_H term is their Coulomb ferromagnetic (Hund's rule) exchange interaction, and

$W = W_{eo} c_{e\downarrow}^\dagger c_{e\uparrow}^\dagger c_{o\uparrow} c_{o\downarrow} + W_{eo}^* c_{o\downarrow}^\dagger c_{o\uparrow}^\dagger c_{e\uparrow} c_{e\downarrow}$ is a small but nonzero pair hopping term. To fix the model parameters from the first principles DFT input, we require the scattering phase shifts of the model Hamiltonian at the Hartree Fock (mean-field) level to reproduce the phase shifts of the *ab initio* scattering calculation for the full system. The physical picture behind this type of matching is the local moment regime of the Anderson impurity model; since spin-polarized DFT and Hartree Fock provide comparable mean-field descriptions of the local moment regime, we can reliably infer the model parameters by requiring them to give the same phase shifts. With four total phase shifts from the two channels and two spin polarizations, these conditions determine the four model parameters ϵ_e, ϵ_o, U_e and U_o. To fix the remaining parameters U_{eo}, J_H and W_{eo}, we make use of relationships between the interaction parameters that are exact for the isolated molecule (*SI Text*) and which should still apply to the adsorbed molecule owing to its gentle physisorption. The resulting parameters (*Table S2*) provide all the ingredients we need for a many body calculation of the spectral function and Kondo conductance anomaly.

NRG Results

The two-orbital Anderson model, Eq (1), is solved by NRG [34–36]; details are given in *Materials and Methods*. For tilted NO adsorbed at the on-top site, the solution indicates a competition between even and odd $2\pi^*$ orbitals. The $2\pi^*_e$ is much more hybridized with the Au surface, whereas the $2\pi^*_o$ has a lower bare energy, and it is thus unclear at the outset which of the two will host the Kondo resonance. We find, somewhat surprisingly, that at the fixed point the least hybridized, odd orbital is the winner, its spectral function displaying the Kondo resonance shown in Fig. 3E. By occupying the $2\pi^*_o$ more substantially than the $2\pi^*_e$, NRG inverts the mean-field orbital occupations initially obtained in DFT. At $T = 0$ K, the NRG orbital occupations are $n_o = 0.83$ and $n_e = 0.34$, while the DFT occupations were $n_o = 0.44$ and $n_e = 0.65$. This exemplifies a situation of more general interest, showing that quantum fluctuations may cause one channel, even one predominant in mean field, to give way to another.

As a general note of caution we should stress that our Anderson model is in a regime where the parameter dependence of the Kondo temperature, lineshape, and orbital population balance, is rather critical. Kondo temperatures are particularly difficult to predict, given their exponential dependence on parameters. At the same time, the accuracy of the DFT electronic structure and phase shifts near ϵ_F, which determine those parameters, is limited by inaccuracies and approximations, including in particular self-interaction errors. The Kondo temperature increases by a factor of three if the hybridization is increased by 20% or the orbital energy splitting $\epsilon_e - \epsilon_o$ is decreased by only 50 meV. Further decreasing $\epsilon_e - \epsilon_o$ leads to a rather abrupt transition—via charge transfer from $2\pi^*_o$ to $2\pi^*_e$—to a state with a broad resonant level
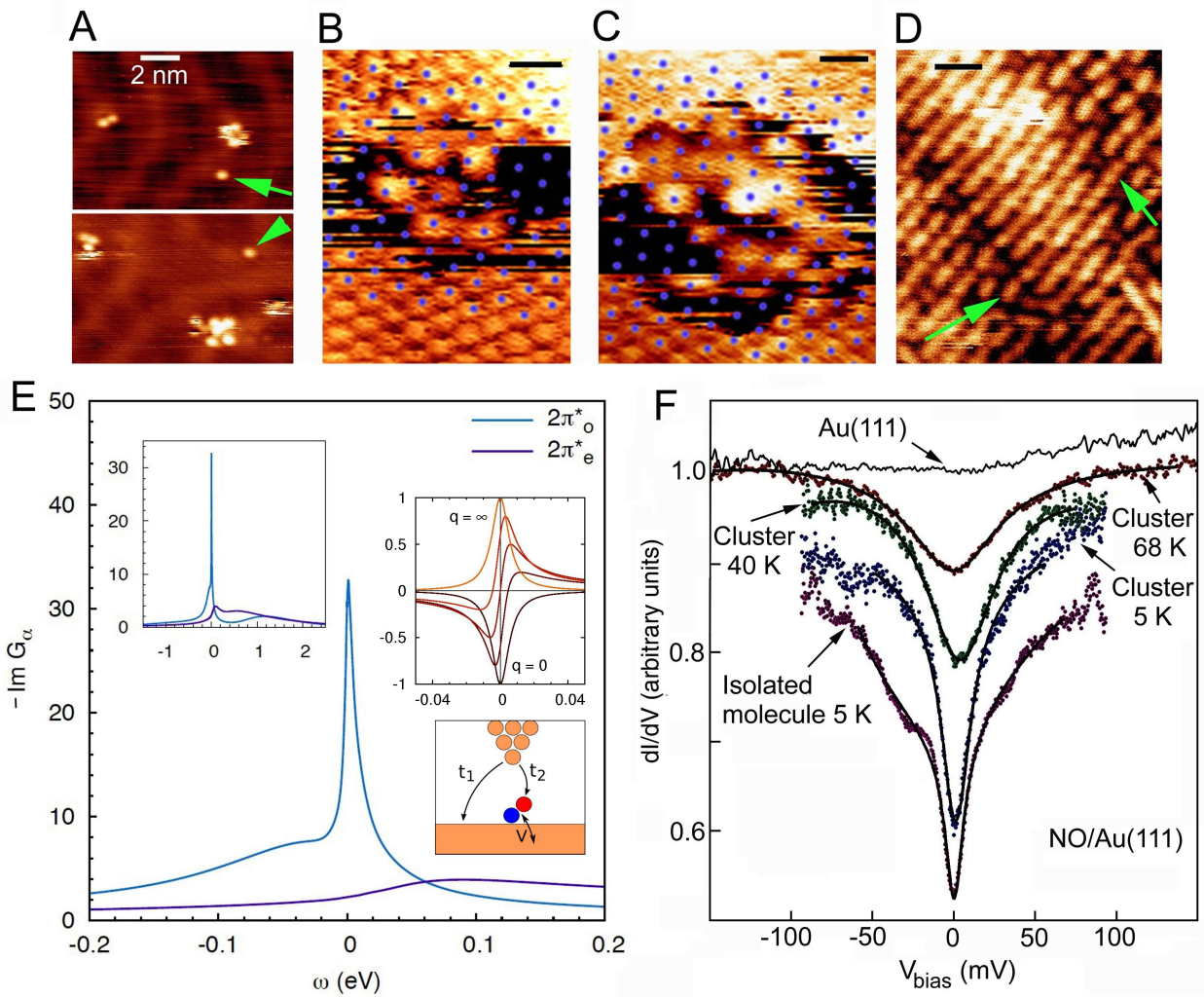
FIG. 3: STM/STS images and spectra, all obtained with clean Au tips except for B,C. (A) Isolated NO molecules (see arrows) and small NO clusters on Au(111) at 5 K. (B,C) Two small NO clusters formed from a few molecules (in the center of the figure) and substrate Au atoms (at the edges of the figure) imaged with a molecule on the STM tip; the Au lattice is marked by blue dots. Most of the molecules are on-top. The bar on the top is 0.5 nm. (D) Filled state STM image ($V_{bias} = -60$ mV) of an ordered single NO layer obtained after annealing at 70 K. The layer is made up of rows of units with a dumbbell shape that is consistent with the shape of the filled $2\pi_o^*$ orbital. The arrows point to two of these units. (E) NRG spectral functions for the $2\pi^*$ orbitals of NO at the on-top adsorption site calculated at 5 K with ab initio parameters from Table S2. Insets: spectral function (left), Fano lineshapes (top right) and interfering tunneling paths t_1 and t_2 (bottom right). (F) Tunneling spectra of isolated molecules and small clusters at 5 K and clusters at 40 K and 68 K showing the Kondo dip. The spectra are shifted vertically for clarity. The solid lines are fits with the Frota function [37].

at ϵ_F rather than a Kondo resonance. We stick here to the results predicted by our straightforward protocol, without adjustments or data fitting.

Experimental STM/STS Results

To verify the theoretical predictions just presented, we carried out STM measurements of NO adsorbed on Au(111). Submonolayer NO was dosed on a reconstructed Au(111) surface at 30 K, and the sample was then cooled to 5 K. STM images acquired with tunneling currents below 10^{-11} A show that the molecules adsorb preferentially at the fcc elbows of the gold herringbone surface reconstruction as isolated units or small

disordered clusters at low coverage—below about 0.05 monolayers—and form large disordered clusters at higher coverage. The images of small clusters in Figs. 3B-C indicate that the largest proportion of molecules adsorb on-top, in agreement with the theoretical prediction. The average nearest neighbor NO-NO distance in the clusters is about 0.5 nm. After annealing at 70 K, the molecules form ordered islands with a variety of metastable lattices with unit vectors between 0.35 and 0.60 nm. The angle between the unit vectors of the molecular lattices and those of the gold surface is between 0 and 30 degrees. The structures are either incommensurate with the sub-

strate or have a large unit cell with several inequivalent molecules, suggesting that the NO-NO interaction prevails over the NO-Au interaction. The NO lattice shown in Fig. 3D is formed by units that have a dumbbell appearance in the filled-state STM images. This shape is consistent with the charge distribution of the $2\pi_o^*$ orbital of the tilted molecule (Fig. S1) and supports the results of the NRG calculations that predict this state is preferentially filled.

STM spectra measured on isolated NO molecules, small disordered clusters, large disordered clusters and ordered NO lattices all display similar dip-shaped conductance anomalies centered at the Fermi level, as shown in Figure 3F. For isolated molecules, whose mobility at 5 K was too high to acquire images with enough resolution to detect the predicted on-top adsorption state and tilt angle, the HWHM of the dip is about 12 ± 4 meV at 5 K with an amplitude that is $\sim 25\%$ of the background conductance. For NO clusters and lattices, the dip HWHM is 16 ± 4 meV at 5 K and depends on the position of the molecule. In addition to the zero bias dip, shoulders at ± 30 meV are visible in the spectra taken over the isolated molecule but not over clusters (Fig. 3F). We have not been able to determine whether these inelastic features are of vibrational or electronic origin, but the symmetric displacement of the shoulders with respect to zero bias, as well as their disappearance in clusters, is suggestive of a vibrational origin. By DFT calculations we find vibrational eigenmodes with frequencies of 25 and 42 meV in the correct range. Spin transitions and anisotropy are not expected for a spin 1/2. Hypothetically, electronic states might offer an alternative explanation, the lower Hubbard band of the $2\pi_o^*$ state, visible just below Fermi in the NRG spectra (Fig. 3E), corresponding to the left shoulder, and the empty $2\pi_e^*$ state forming a resonance above Fermi, to the right shoulder. Altogether, an electronic explanation seems less likely.

No other sharp structures were observed between -0.8 and 0.8 eV from the Fermi level as shown in *Fig. S2* and described in *SI Text*. In particular, the large step at -0.45 eV corresponding to the bottom of the clean Au(111) surface state band is absent in the spectra measured over molecules, indicating that free surface state electrons are pushed out by the NO molecule, to become detectable again in spectra 1-2 nm away. Although surface states are repelled, nevertheless their tails are expected to extend up to and hybridize with the NO radical.

To further confirm the Kondo nature of the observed zero bias STM anomaly, the temperature dependence of the half width at half maximum of the dip was measured and is shown in Figure 4. For each temperature, the lineshape was fit with an asymmetric version [38] of the Frota function [37] with asymmetry parameter $\phi = \pi$. By 70 K, the HWHM has grown to 40-50 meV and the amplitude has decreased from $\sim 25\%$ to $\sim 10\%$ of the background. Due to the high mobility of the isolate molecules at high temperature and the ensuing difficulty of acquiring spectra for them, all data presented for $T > 5$ K were taken
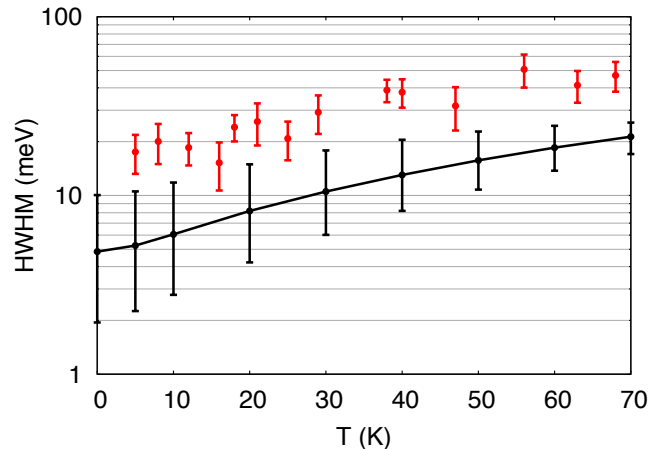

FIG. 4: Temperature dependence of the HWHM of the Kondo resonance from experiment (red) and NRG calculations (black) based on the ab initio parameters for the on-top adsorption geometry (*Table S2*). Experimental error bars indicate the standard deviation calculated from a collection of spectra on different NO molecules. Spectra were measured on at least 10 different molecules at each temperature. The error bars on the theoretical curve represent the uncertainty corresponding to a $\pm$ 20 percent uncertainty in the hybridization linewidth; uncertainty from other parameters is not depicted. Model parameter SDs are reported in Table S2.

on NO islands. The temperature induced broadening and attenuation of the dip is intrinsic because it is about a factor of five larger than the effect of the change of the experimental resolution of STS at high temperature related to the broadening of the Fermi distribution of the tip, corresponding to a HWHM of about 10 meV at 68 K. The large intrinsic broadening rules out inelastic tunneling (vibrational or electronic excitations) as the main origin of the dip. The Kondo temperature ~ 43 K, extracted from the low temperature limit of the Frota linewidth parameter Γ_K, is about a factor of three larger than our unbiased theoretical prediction. This level of discrepancy is not surprising in view of the exponential sensitivity of the Kondo temperature to the impurity parameters, and of the self-interaction errors generally affecting the first principles DFT calculations.

Actually, a theoretical underestimate of the Kondo temperature is not unexpected, since the hybridization with gold surface states, as was mentioned above, is not completely accounted for in our calculations. Despite these deficiencies, the overall, unbiased theoretical results are gratifyingly reproduced, and so is the evolution of the zero bias anomaly with temperature, as shown in Fig. 4. The experimental offset of the center of the dip from the Fermi energy, less than 2 meV, is much less than the width, indicating that the parent level of the Kondo resonance is indeed nondegenerate. That provides an indirect and yet strong confirmation that the NO molecule is tilted, for if the $2\pi^*$ levels were degenerate the Kondo peak would be shifted above the Fermi energy to satisfy

the Friedel sum rule [39]. The data do not clearly establish if the symmetry of the Kondo orbital is odd as predicted, and that remains to be verified, e.g., by photoemission spectroscopy.

Finally, the observed Fano conductance lineshape (inset Fig. 3E), a $q \simeq 0$ dip rather than $q \simeq \infty$ as predicted by the impurity spectral function, indicates that direct tunneling into the molecular $2\pi^*$ states (t_2 in inset Fig. 3E) is dominated by another tunneling channel (t_1). As STS indicates, the NO molecule is fully immersed in the Au(111) surface states, whose wave functions extend far out into the vacuum, reaching out to the STM tip. Because surface states do not represent a bulk screening channel, they are not included in our scattering calculations. Since the surface states are nonetheless involved and provide a free electron reservoir for Kondo screening, their local density of states near the molecule will show a dip at the Fermi energy, complementary to the calculated bare NO spectral function peak. As observed in the Kondo STM conductance anomalies of many other adsorbed magnetic atoms, and as generally discussed by Ujsaghy et al. [40], dI/dV spectra are strongly modified, in our case very plausibly dominated, by direct tunneling into nearby metal surface states, specularly reversing the intrinsic Kondo anomaly.

Conclusions and Outlook

We have described how the Kondo parameters and resulting zero bias STM conductance anomaly of an adsorbed molecular radical can be predicted from first principles, with features that compare reasonably well with a subsequent experiment. To do so, we employed NO as the simplest spin 1/2 molecular radical capable of forming a Kondo screening cloud when adsorbed on a gold surface. The discrepancies between the calculated Kondo temperature and lineshape, which we did not try to amend in any way, and the measured ones are quite instructive, highlighting in particular the need to fully incorporate the metal surface states in future calculations. The delicate renormalization group flow towards the least hybridized, odd symmetry $2\pi_o^*$ state also appears as an instructive many body effect, and remains a prediction to be verified. The magnetic field splitting of the Kondo anomaly, presently academic in view of the large value of T_K, could easily be calculated if need be.

The protocol implemented here for NO/Au(111) in a specific STM geometry is of more general applicability and can be applied to different molecular radicals and different STM and break junction geometries, where the influence of structural or mechanical deformations could be explored. As an overall result, the DFT+NRG approach demonstrates enough predictive power to be useful in the *a priori* evaluation of the conductance characteristics of molecular radical nanocontacts, thus providing a theoretical asset of considerable technological relevance.

Materials and Methods

Density functional theory calculations in the generalized gradient approximation of Perdew, Burke and Ernzerhof

[8] were performed with Quantum Espresso [42], a plane wave pseudopotential electronic structure package. The NO/Au(111) adsorption geometry was determined using the slab method in a 3×3 surface supercell with a vacuum layer of 16.9 Å. Scattering calculations were carried out with pwcond [32] in a 3×3 supercell with a vacuum layer of 8.4 Å, in correspondence with the experimental tip height of ∼10 Å. Brillouin zone integrations were performed on a 6×6×2 k-point mesh with a smearing width of 0.002-0.010 Ry. Plane wave cut-offs were 30 Ry for the wave function and 360 Ry for the charge density. As detailed in (SI Text), Hubbard interactions were applied to the d states of Au (U=1.5 eV) and the p states of N and O (U=1.0 eV).

Numerical renormalization group calculations were carried out with NRG Ljubljana [35] employing the z-averaging technique [36], the full density matrix approach [43] and the self-energy trick [44]. The logarithmic discretization parameter was chosen to be $\Lambda = 4$, and a maximum of 2000 states (not counting multiplicities), corresponding to roughly 5000 total states, were kept at each iteration. Spectral functions were obtained by log-gaussian broadening [45] and at finite temperature with a kernel that interpolates between a log- gaussian at high energy and regular gaussian at low energy [43].

The dI/dV spectra were measured with a clean Au tip by the lock-in technique applying a 3 meV modulation to the bias voltage and using a maximum current of 3×10^{-11} A to avoid tip induced modification of the adsorption geometry. NO molecules were easily displaced at higher tunneling currents at 5 K and were mobile at temperatures above 20-30 K. The gold lattice and molecules could be resolved simultaneously only once, Figs. 3B and C, when an unknown molecule adsorbed on the tip. The horizontal stripes in Figs. 3B and C are caused by temporary detachments or shifts of this molecule. The broadening of the tunneling spectra caused by the finite modulation voltage is taken into account in the fit of the measured spectra by calculating the convolution of the Frota function with $\sqrt{1 - (V/V_{\mathrm{pp}})^2}$, where V_{pp} is the peak- to-peak value of the modulation voltage and V is the bias. This function represents the response of the STS spectroscopy with a sinusoidal modulation of the bias and a lock-in amplifier to a delta function-like density of states. The effect of the thermal broadening of the Fermi distribution in the tip at high temperature was taken into account by computing the convolution of the Frota function with the derivative of the Fermi distribution.

[1] Aviram A, Ratner MA (1974) Molecular rectifiers. *Chem Phys Lett* 29(2):277-283.

[2] Reed MA, et al. (1997) Conductance of a molecular junction. *Science* 278:252-254.

[3] Joachim C, Gimzewski JK, Aviram A (2000) Electronics using hybrid-molecular and mono-molecular devices. *Nature* 408:541-548.

[4] Hewson A (1993) *The Kondo Problem to Heavy Fermions* (Cambridge Univ Press).

[5] Madhavan V, Chen W, Jamneala T, Crommie MF, Wingreen NS (1998) Tunneling into a single magnetic atom: spectroscopic evidence of the Kondo resonance. *Science* 280:567-569.

[6] Li J, Schneider W-D, Berndt R, Delley B (1998) Kondo scattering observed at a single magnetic impurity. *Phys Rev Lett* 80(13):2893-2896.

[7] Parks JJ, et al. (2010) Mechanical control of spin states in spin-1 molecules and the under screened Kondo effect. *Science* 328:1370-1373.

[8] Scott GD, Natelson D (2010) Kondo resonances in molecular devices. *ACS Nano* 4(7):3560-3579.

[9] Wahl P, Diekhöner L, Wittich G, Vitali L, Schneider MA, Kern K (2005) Kondo effect of molecular complexes at surfaces: ligand control of the local spin coupling. *Phys Rev Lett* 95:166601.

[10] Zhao A, et al. (2005) Controlling the Kondo effect of an adsorbed magnetic ion through its chemical bonding. *Science* 309:1542-1544.

[11] Iancu V, Deshpande A, Hla S-W (2006) Manipulating Kondo temperature via single molecule switching. *Nanolett* 6(4):820-823.

[12] Jiang Y, Zhang YN, Cao JX, Wu RQ, Ho W (2011) Real-space imaging of Kondo screening in a two-dimensional O_2 lattice. *Science* 333:324-328.

[13] Mugarza A, et al. (2011) Spin coupling and relaxation inside molecule-metal contacts. *Nat Commun* 2:490.

[14] Müllegger S, Rashidi M, Fattinger M, Koch R (2012) Interactions and self-assembly of stable hydrocarbon radicals on a metal support. *J Phys Chem C* 116: 22587-22594.

[15] Müllegger S, Rashidi M, Fattinger M, Koch R (2013) Surface-supported hydrocarbon π radicals show Kondo behavior. *J Phys Chem C* 117:5718-5721.

[16] Zhang Y-H, et al. (2013) Temperature and magnetic field dependence of a Kondo system in the weak coupling regime. *Nature Comm* 4:2110.

[17] Park J, et al. (2002) Coulomb blockade and the Kondo effect in single-atom transistors. *Nature* 417:722-725.

[18] Parks JJ, et al. (2007) Tuning the Kondo effect with a mechanically controllable break junction. *Phys Rev Lett* 99:026601.

[19] Osorio EA, et al. (2007) Electronic excitations of a single molecule contacted in a three-terminal configuration. *Nano Lett* 7(11):3336-3342.

[20] Lucignano P, Mazzarello R, Smogunov A, Fabrizio M, Tosatti E (2009) Kondo conductance in an atomic nanocontact from first principles. *Nature Mater* 8:563-567.

[21] Baruselli PP, Smogunov A, Fabrizio M, Tosatti E (2012) Kondo effect of magnetic impurities on nanotubes. *Physica E* 44:1040.

[22] Baruselli PP, Smogunov A, Fabrizio M, Tosatti E (2012) Kondo effect of magnetic impurities in nanotubes. *Phys Rev Lett* 108:206807.

[23] Costi TA, et al. (2009) Finding the right spin model for iron impurities in gold and silver. *Phys Rev Lett* 102:056802.

[24] Jacob D, Haule K, Kotliar G (2009) Kondo effect and conductance of nanocontacts with magnetic impurities. *Phys Rev Lett* 103:16803.

[25] Dias da Silva LGGV, Tiago ML, Ulloa SE, Reboredo FA, Dagotto E (2009) Many-body electronic structure and Kondo properties of cobalt-porphyrin molecules. *Phys Rev B* 80:155443.

[26] Surer B, Troyer B, Werner B, Wehling TO, Läuchli AM, Wilhelm A, Lichtenstein AI (2012) Multiorbital Kondo physics of Co in Cu hosts. *Phys Rev B* 85:085114.

[27] Yoshimori A (1995) Does a localized spin of adsorbed NO survive on Cu(111)? *Surf Sci* 342:L1101-L1103.

[28] Pérez Jigato M, King DA, Yoshimori A (1999) The chemisorption of spin polarized NO on Ag{111}. *Chem Phys Lett* 300:639-644.

[29] Wäckerlin C, et al. (2010) Controlling spins in adsorbed molecules by a chemical switch. *Nature Commun* 1:61.

[30] Barth JV, Brune H, Ertl G, Behm RJ (1990) Scanning tunneling microscopy observations on the reconstructed Au(111) surface: atomic structure, long-range super-structure, rotational domains, and surface defects. *Phys Rev B* 42:9307-9318.

[31] McClure SM, Kim TS, Stiehl JD, Tanaka PL, Mullins CB (2004) Adsorption and reaction of nitric oxide with atomic oxygen covered Au(111). *J Phys Chem B* 108(46): 17952.

[32] Smogunov A, Dal Corso A, Tosatti E (2004) Ballistic conductance of magnetic Co and Ni nanowires with ultrasoft pseudopotentials. *Phys Rev B* 70: 045417.

[33] Forster F, Benounan A, Reinert F, Grigoryan VG, Springborg M (2007) *Surf Sci* 601:5595-5604.

[34] Bulla R, Costi TA, Pruschke T (2008) Numerical renormalization group method for quantum impurity systems. *Rev Mod Phys* 80:395-450.

[35] Žitko R, NRG Ljubljana, http://nrgljubljana.ijs.si.

[36] Žitko R, Pruschke T (2009) Energy resolution and discretization artifacts in the numeric renormalization group. *Phys Rev B* 79:085106.

[37] Frota HO (1992) Shape of the Kondo resonance. *Phys Rev B* 45: 1096-1099.

[38] Prüser H, Wenderoth M, Weismann A, Ulbrich RG (2012) Mapping itinerant electrons around Kondo impurities. *Phys Rev Lett* 108:166604.

[39] Choi M-S, López R, Aguado R (2005) SU(4) Kondo effect in carbon nanotubes. *Phys Rev Lett* 95:067204.

[40] Újsághy O, Kroha J, Szunyogh L, Zawadowski A (2000) Theory of the Fano resonance in the STM tunneling density of states due to a single Kondo impurity. *Phys Rev Lett* 85:2557-2560.

[41] Perdew JP, Burke K, Ernzerhof M (1996) Generalized gradient approximation made simple. *Phys Rev Lett* 77:3865-3868.

[42] Giannozzi P, et al. (2009) Quantum Espresso: a modular and open-source software project for quantum simulations of materials. *J Phys: Condens Matter* 21: 395502.

[43] Weichselbaum A, von Delft J (2007) Sum-rule conserving spectral functions from the numerical renormalization group. *Phys Rev Lett* 99:076402.

[44] Bulla R, Hewson AC, Pruschke T (1998) Numerical renormalization group calculations for the self-energy of the impurity Anderson model. *J Phys: Condens Matt* 10: 8365-8380.

[45] Bulla R, Costi TA, Vollhardt D (2001) Finite-temperature numerical renormalization group study of the Mott transition. *Phys Rev B* 64:045103.

[46] Momma K, Izumi F, VESTA visualization program, http://jp-minerals.org/vesta.

[47] Adopting Wilson's definition, the Kondo temperature $T_{K,W}$ is inferred from $\Delta_{\mathrm{HWHM}} \approx 4.6 k_B T_{K,W}$ [36], where the HWHM is extracted from the linewidth Γ_K obtained from a Frota lineshape fit [37].

Supporting Information

R. Requist, et al.

SI Text

First principles electronic structure calculations

Density functional theory calculations of NO adsorption were performed using the slab method with 3-7 gold layers and a 3×3 hexagonal supercell of the unreconstructed Au(111) surface, corresponding to 1/9 monolayer coverage. This cell was large enough to reduce the interaction between periodic images of the NO molecule to a negligible level. Selected calculations were repeated with 2×2, $2\sqrt{3} \times \sqrt{3}$ and $2\sqrt{3} \times 2\sqrt{3}$ cells to verify convergence. The unreconstructed Au(111) surface is expected to be a good approximation to the face-centered cubic (fcc) regions of the well-known $22 \times \sqrt{3}$ "herringbone" reconstruction, where the experimental measurements were performed. For calculations of the adsorption energy, the vacuum layer was set to 16.9 Å, while for calculations of the scattering phase shifts, it was reduced to 8.4 Å, corresponding to the experimental tip height. The latter value was large enough that the shape of the tip (cf. Fig. 1 of the main article) had a negligible effect on the adsorption geometry and hybridization linewidths. Hence, the scattering calculations were performed without any model for the tip, essentially using the bottom of the slab as a broad distant probe.

The unreconstructed Au(111) surface presents 4 distinct high-symmetry adsorption sites – fcc, hexagonal close packed (hcp), bridge and on-top. For each site, all the coordinates of NO and the two highest layers of gold were fully optimized. By subsequently applying constraints to the Au atoms, it was found that only the relaxation of the Au atoms nearest to N had a significant effect on the results, and therefore in the scattering calculations we fixed all Au atoms to their bulk positions, except the 1, 2, or 3 Au atoms nearest N in the case of top, bridge, and hollow site adsorption, respectively. At the top site, the Au atom directly beneath N, which we label as Au_{top}, is pulled out of the surface by 0.11 Å, enhancing the interaction between the NO $2\pi^*$ molecular orbitals and an *spd* hybrid orbital (mainly d_{z^2}) of Au_{top}.

Table S1 summarizes our *ab initio* results for gas phase NO and NO/Au(111), including the adsorption energy E_{ads}, magnetic moment μ, NO bond length d_{NO}, AuN bond length d_{AuN}, the stretching frequency ν_{NO}, and electric dipole moment calculated with GGA+U. The magnetic moment is reported for the entire cell, including the small induced magnetization on gold. The surface-adsorbate electric dipole moment was calculated by applying a sawtooth-shaped potential along the z direction. At the top site, NO was found to tilt away from the upright configuration, giving a Au_{top}-N-O angle of 122.4°, in agreement with earlier calculations [1]. The tilting, which accounts for a large part of the adsorption energy, is crucial for the present study because it alters the Kondo physics by lifting the degeneracy of the $2\pi^*$ orbitals. The molecule tilts toward one of the six nearest neighbor surface gold atoms of Au_{top}. For definiteness, we shall take the molecule to tilt in the positive x direction, so that the tilt plane is the xz plane. The degenerate $2\pi^*$ orbitals split into two orbitals that we label as $2\pi_e^*$ and $2\pi_o^*$ according to their symmetry (even or odd) with respect to reflection through the tilt plane. Full geometry optimization shows that the tilt plane undergoes a small azimuthal rotation of 8.6° around the surface normal. The order of magnitude of the calculated adsorption energies agrees with an estimate of 400 meV from temperature programmed desorption spectroscopy [4] and the results of a comprehensive study [1] of NO adsorption on metal surfaces, although the site dependence differs. We are not aware of any further experimental data for NO/Au(111), but our calculations of the molecule in vacuum (Table S1) are in good agreement with gas phase measurements. The calculated ionization energy of NO, 9.007 eV, is also fairly close to the experimental value 9.27483 ± 0.00005 eV [5]. The work function of gold, calculated with a 24-layer slab with 24 Å of vacuum, is 5.19 eV and compares favorably with the experimental value 5.31 eV [6].

In view of the weak adsorption energy, selected calculations were performed with the following four functionals in order to judge the sensitivity of the results to the choice of exchange-correlation functional: i) the local (spin) density approximation (LDA) of Perdew and Zunger [7], ii) the generalized gradient approximation (GGA) of Perdew, Burke and Ernzerhof [8], iii) the Heyd-Scuseria-Ernzerhof (HSE) hybrid functional [9], and iv) a modified version [10] of the Vydrov-Van Voorhis (VV10) functional [11] describing van der Waals interactions. The LDA approximation, known to be overbonding for molecules on surfaces, was found to be inadequate, causing NO to demagnetize. The VV10 functional increased the adsorption energy uniformly for all sites, yielding 540, 380 and 360 meV for the on-top, bridge and fcc sites, respectively. Hybrid functionals have been found to give good results for the adsorption of small molecules on metal surfaces [12]; however, since they open a small gap at the Fermi energy in metals, they are potentially problematic when the molecular levels lie close to the Fermi energy, as they do in our case. Moreover, such a gap would cause artifacts in the calculation of the scattering phase shifts. For these reasons, all of the results reported in the main article were obtained with the GGA and GGA+U.

Hubbard interactions $U_N = U_O = 1$ eV were applied to the N and O p orbitals in the GGA+U scheme in order to stabilize the magnetic moment. Similar values have been used for CO to correct the adsorption site preference on Pt(111) [13] and Cu(111) and Cu(001) [14]. We also used Hubbard interactions to correct the energy of the Au d bands, which in LDA and GGA [15, 16] are too high compared with angle-resolved photoemission spectroscopy [17]. We found that the value $U_{Au} = 1.5$ eV

shifts the fully occupied d bands down rigidly by 0.5 eV, bringing them into agreement with experiment, while leaving the sp bands virtually unchanged. This value of U_{Au} was adopted in calculating all quantities in Table S1. The GGA+U scheme has been used in a similar way to correct the d states of Ni in a study of the adsorption of CO and NO/NiO(100) [18, 19].

The projected density of states for the isolated molecule, clean surface and the combined surface-adsorbate system are shown in Figure S1. The most important observation is that the degeneracy of the $2\pi_e^*$ and $2\pi_o^*$ orbitals is broken by the tilting of the molecule, yet both remain partially occupied. The tilting of the molecule away from the upright configuration increases the hybridization of the $2\pi_e^*$ orbital and decreases the hybridization of the $2\pi_o^*$ orbital. As reported in Table S2, the hybridization Γ_e becomes fives times as large as Γ_o for the optimal tilt angle of nearly 60 degrees.

Despite the substantial tilting of the molecule, there is only a relatively weak symmetry breaking in the $2\pi^*$ orbital occupations. One might have expected the $2\pi_e^*$ orbital to be nearly empty, since its bare energy is pushed up by as much as 0.24 eV due to its antibonding interaction with the spd hybrid orbital of Au$_{\text{top}}$. Instead, it is even more occupied than the $2\pi_o^*$ orbital. The $2\pi_e^*$ and $2\pi_o^*$ molecular orbitals have fractional occupation numbers, $n_e = 0.65$ and $n_o = 0.44$, adding up to slightly more than 1, consistent with modest charge transfer from the surface to the molecule. The degeneracy of the 1π orbitals is also lifted by the tilting, but they split in the opposite direction because they lie below rather than above the d states in energy. The lack of distinct symmetry breaking in the $2\pi^*$ orbital occupations might be a spurious result, possibly caused by self-interation error, or it might be a genuine consequence of orbital fluctuations. Hubbard interactions in nitrogen and oxygen are unable to induce a stronger symmetry breaking even though they increase the $2\pi_e^*/2\pi_o^*$ splitting for the spin and orbital symmetry-broken solution in vacuum. It might be possible to achieve orbital symmetry breaking by applying Hubbard-type interactions to molecular orbitals rather than atomic orbitals (cf. Ref. [13]) or in an approach with inherently less self-interaction error such as reduced density matrix functional theory, but we do not pursue these approaches here.

The Blyholder [20] and Hammer-Morikawa-Norskov [21] models, which describe the adsorption of CO on metals in terms of σ donation and π back-bonding, provide a starting point for understanding the bonding interactions between NO and the gold surface, however σ and π are no longer proper symmetries due to the tilting of the molecular axis. Modest back-bonding interactions are visible at the top of the d band ($\sim$2.5 eV below the Fermi energy) in Fig. S1, coinciding with peaks in the Au$_{\text{top}}$ d_{z^2} states. The strong participation of the Au$_{\text{top}}$ d_{z^2} states in the $2\pi_e^*$, 5σ, $1\pi_e$ and 4σ molecular resonances is an important feature of the bonding interaction. There are important differences between the adsorption of NO and CO on noble metals, since NO is an open-shell molecule.

Constructing an Anderson impurity model

An Anderson model representing the hybridization of the $2\pi^*$ molecular orbitals of NO with the Au(111) surface was defined in Eq. **1** of the main article. In specifying the interaction Hamiltonian H_{int}, it is convenient to start from the molecule in vacuum. Since the isolated molecule has cylindrical symmetry, the interactions in the $2\pi^*$ sector depend on only two independent parameters and can be expressed as

$$H_{\text{int}} = \frac{V}{2}N(N-1) - 2J\mathbf{S}^2 + \frac{J}{2}L_z^2, \qquad \text{(S1)}$$

where N is the total number of electrons, $\mathbf{S}$ is the total spin operator, and L_z is the total z component of angular momentum. The two degenerate $2\pi^*$ states, formed from the p_x and p_y orbitals of N and O, can be chosen to be eigenstates of L_z, i.e. $|m = \pm 1\rangle$. The $|m = 0\rangle$ state is not considered because the p_z orbitals, being involved in σ bonding, are far lower ($\sim$7.5 eV) in energy. Since we will be considering the symmetry breaking caused by tilting, we express Eq. (S1) in terms of the $2\pi_x^*$ and $2\pi_y^*$ states, which have nodes in the yz and xz planes, respectively. Using the relations $c_{m=1} = (-c_x - ic_y)/\sqrt{2}$ and $c_{m=-1} = (c_x - ic_y)/\sqrt{2}$, we find

$$H_{\text{int}} = U_x n_{x\uparrow}n_{x\downarrow} + U_y n_{y\uparrow}n_{y\downarrow} + U_{xy}n_x n_y + J_H \mathbf{S}_x\cdot\mathbf{S}_y + W + \beta N, \qquad \text{(S2)}$$

where the U terms are on-site and inter-site Hubbard interactions, the J_H term is a Hund interaction ($\mathbf{S}_\alpha$ is the spin operator for the $2\pi_\alpha^*$ state, *not* the α-component of spin) and W is a double hopping term $W = W_{xy}c_{x\uparrow}^\dagger c_{x\downarrow}^\dagger c_{y\downarrow}c_{y\uparrow} + W_{xy}c_{y\uparrow}^\dagger c_{y\downarrow}^\dagger c_{x\downarrow}c_{x\uparrow}$. The parameters are uniquely determined by (V, J) according to the formulas $U_x = U_y = V + 3J$, $U_{xy} = V - J/2$, $J_H = -6J$, $W_{xy} = -J$ and $\beta = -J/2$.

When the molecule is brought down to the surface in an upright configuration at the on-top, fcc or hcp sites, the crystal field lowers the cylindrical symmetry to C_{3v} symmetry. The degeneracy of the $2\pi^*$ states is preserved and Eqs. (S1) and (S2) remain exact. The tilting of the molecule breaks the symmetry and lifts the $2\pi^*$ degeneracy. The $2\pi_x^*$ orbital evolves into the even $2\pi_e^*$ orbital (see Fig. 2 of the main article) that hybridizes strongly with the surface. The $2\pi_y^*$ orbital becomes the odd $2\pi_o^*$ orbital with much weaker hybridization. Equation (S2) remains a valid description of interactions in the $2\pi^*$ sector; however, since the $2\pi_e^*$ and $2\pi_o^*$ orbitals are hybridized with the surface, the interaction parameters will no longer have exactly the same relationship with (V, J) that they have in cylindrical symmetry.

For tilted NO at the on-top site, there were not enough *ab initio* data to fit all of the parameters in Eq. (S2), so we have taken the following strategy. We have fit the parameters that are most sensitive to the tilting, namely ϵ_α and U_α, by matching the spin-symmetry broken mean-field $\epsilon_{\alpha\sigma}$ of the Anderson model to $\epsilon_{\alpha\sigma}^{DFT}$ inferred from

the resonances in the *ab initio* phase shifts. The hybridization linewidths $2\Gamma_\alpha$ were calculated by fitting the resonances in the scattering phase shifts to the following functional form

$$\eta_{\alpha\sigma}(\epsilon) = \frac{\pi}{2} + \arctan\frac{\epsilon - \epsilon_{\alpha\sigma}}{\Gamma_\alpha} + \delta_\alpha, \qquad \text{(S3)}$$

where δ_α is a constant shift attributable to potential scattering. An example of the fitting is shown in Fig. S2. The Hund interaction J_H was set equal to its value for gas phase NO, and the remaining parameters U_{eo} and W_{eo} were assumed to have the same relationship to V and J that they have in cylindrical symmetry (as in gas phase). In this way, all model parameters can be fit reliably, and we obtain the results in Table S2.

For upright NO at the bridge site, the symmetry is lowered to C_{2v}. The $2\pi^*_{e/o}$ state is defined to be the state that is even/odd with respect to the plane containing NO and the two nearest neighbor Au atoms. The interaction parameters were approximated the same way as for the on-top site.

Symmetry between the $2\pi^*_{x/y}$ states is preserved for upright NO at the fcc site. The interaction parameters were approximated the same way as for the on-top site; however, since the occupied (majority spin) level $\epsilon^{DFT}_{\alpha\uparrow}$ is degenerate and therefore pinned to the Fermi energy, we obtained a more stable fit for ϵ_α by requiring charge consistency between DFT and NRG, i.e. $n^{DFT}_\alpha = n^{NRG}_\alpha$.

Scanning tunneling spectroscopy

The densities of states measured with a clean Au tip over NO molecules and over the clean Au(111) surface several nm away from the molecules is shown in Fig. S3 for an extended energy range around the Fermi energy. The step at about -0.45 eV on the gold surface marks the bottom of the surface state band [22]. The surface states cannot be detected on top of the NO molecules and gradually vanish when the tip approaches the molecules. The only sharp feature in the NO spectrum above the noise level is the zero-bias dip. The broad and weak bumps at about -0.15 eV and 0.3 eV approximately coincide with the shoulders of the spectral functions of Fig. 3F of the main article.

[1] Gajdos M, Hafner J, Eichler A (2006) *Ab initio* density-functional study of NO on close-packed transition metal and noble metal surfaces: I. molecular adsorption *J Phys: Condens Matter* 18:13-40.

[2] Nakamoto K (1986) *Infrared and Raman Spectra of Inorganic and Coordination Compounds* (Wiley, New York).

[3] Hoy AR, Johns JWC, McKellar ARW (1975) Stark spectroscopy with the CO laser: dipole moments, hyperfine structure, and level crossing effects in the fundamental band of NO. *Can J Phys/Rev Can Phys* 53:2029-2039.

[4] McClure SM, Kim TS, Stiehl JD, Tanaka PL, Mullins CB (2004) Adsorption and reaction of nitric oxide with atomic oxygen covered Au(111). *J Phys Chem B* 108:17952.

[5] Reiser G, Habenicht W, Müller-Dethlefs K, Schlag EW (1988) The ionization energy of nitric oxide. *Chem Phys Lett* 152:119-123.

[6] Michaelson HB (1977) The work function of the elements and its periodicity. *J Appl Phys* 48:4729-4733.

[7] Perdew JP, Zunger A (1981) *Phys Rev B* 23:5048-5079.

[8] Perdew JP, Burke K, Ernzerhof M (1996) Generalized gradient approximation made simple. *Phys Rev Lett* 77:3865-3868.

[9] Heyd J, Scuseria GE, Ernzerhof M (2003) Hybrid functionals based on a screened Coulomb potential. *J Chem Phys* 118:8207-8215.

[10] Sabatini R, Gorni T, de Gironcoli S (2013) Nonlocal van der Waals density functional made simple and efficient. *Phys Rev B* 87:041108.

[11] Vydrov OA, Van Voorhis T (2010) Nonlocal van der Waals functional: the simpler the better. *J Chem Phys* 133:244103.

[12] Wang Y, de Gironcoli S, Hush NS, Reimers JR (2007) Successful a priori modeling of CO adsorption on Pt(111) using periodic hybrid density functional theory. *J Am Chem Soc* 129:10402-10407.

[13] Kresse G, Gil A, Sautet P (2003) Significance of single-electron energies for the description of CO on Pt(111). *Phys Rev B* 68:073401.

[14] Gajdos M, Hafner J (2005) CO adsorption on Cu(111) and Cu(001) surfaces: improving site preference in DFT calculations. *Surf Sci* 590:117-126.

[15] Takeuchi N, Chan CT, Ho KM (1991) Au(111): a theoretical study of the surface reconstruction and the surface electronic structure. *Phys Rev B* 43:13899-13906.

[16] Mazzarello R, Dal Corso A, Tosatti E (2008) Spin-orbit modifications and splittings of deep surface states on clean Au(111). *Surf Sci* 602:893-905.

[17] Kevan SD, Gaylord RH (1987) High-resolution photoemission study of the electronic structure of the noble-metal (111) surfaces. *Phys Rev B* 36:5809-5818.

[18] Rohrbach A, Hafner J, Kresse G (2004) Molecular adsorption on the surface of strongly correlated transition-metal oxides: a case study for CO/NiO(100). *Phys Rev B* 69: 075413.

[19] Rohrbach A, Hafner J (2005) Molecular adsorption of NO on NiO(100): DFT and DFT+U calculations. *Phys Rev B* 71:045405.

[20] Blyholder G (1964) Molecular orbital view of chemisorbed carbon monoxide. *J Phys Chem* 68:2772-2777.

[21] Hammer B, Morikawa Y, Norskov JK (1996) CO chemisorption at metal surfaces and overlayers. *Phys Rev Lett* 76:2141-2144 (1996).

[22] Chen W, Madhavan V, Jamneala T, Crommie MF (1999) Scanning Tunneling Microscopy Observation of an Electronic Superlattice at the Surface of Clean Gold. *Phys Rev Lett* 80(7):1469-1472.
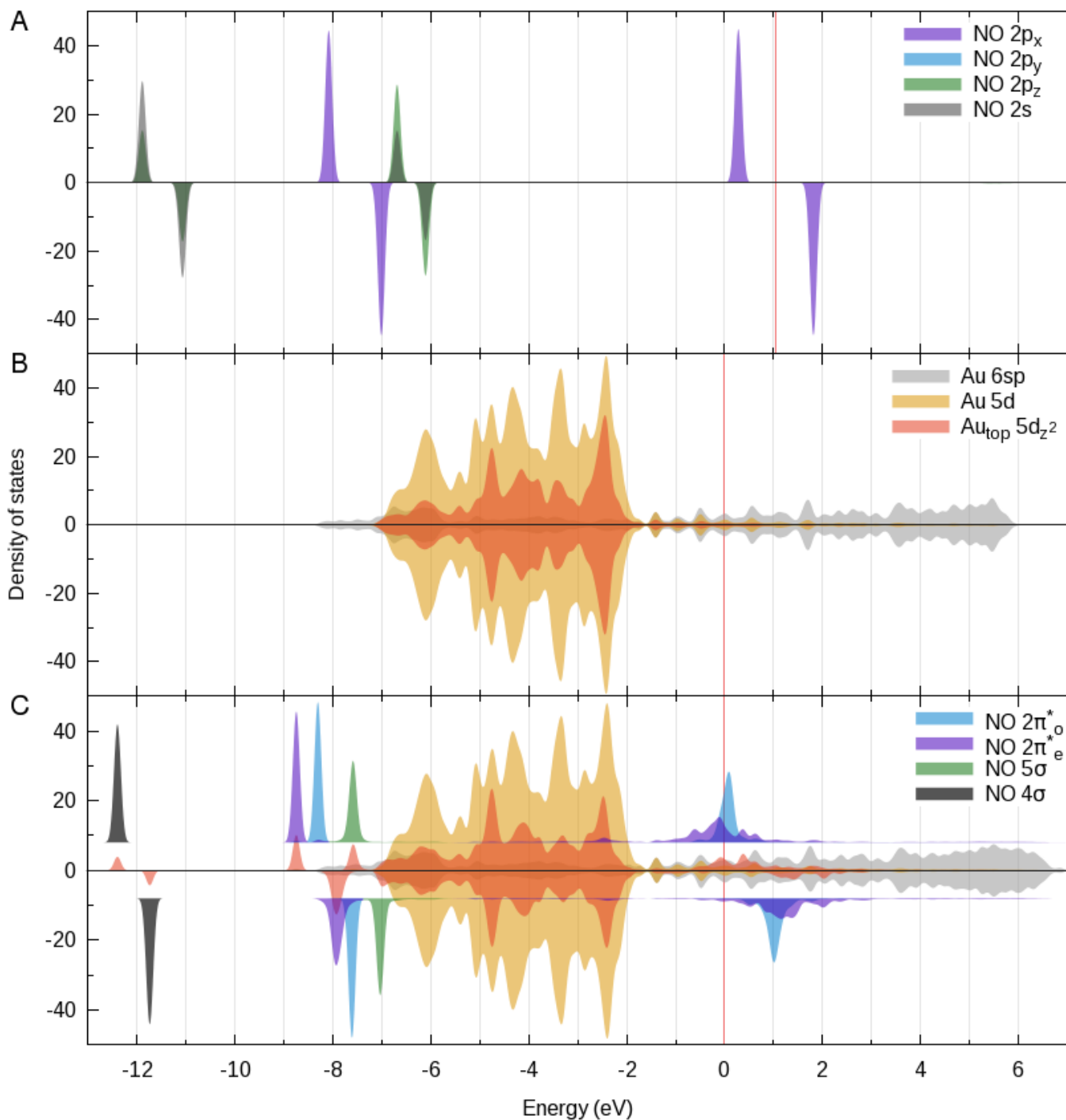
FIG. S1: Projected density of states of (A) Gas phase NO, (B) 3-layer Au(111) slab, and (C) NO/Au(111) slab system. Energies have been shifted so as to align the vacuum levels of all systems; vertical red lines indicate the respective Fermi energies. Artificial gaussian broadening of 0.10 eV is used. NO $2p_x$ and $2p_y$ orbitals are degenerate in gas phase. The density of states of the $2\pi^*$ orbitals are calculated from weighted sums of N and O p_x and p_z orbitals, corresponding to the tilting.
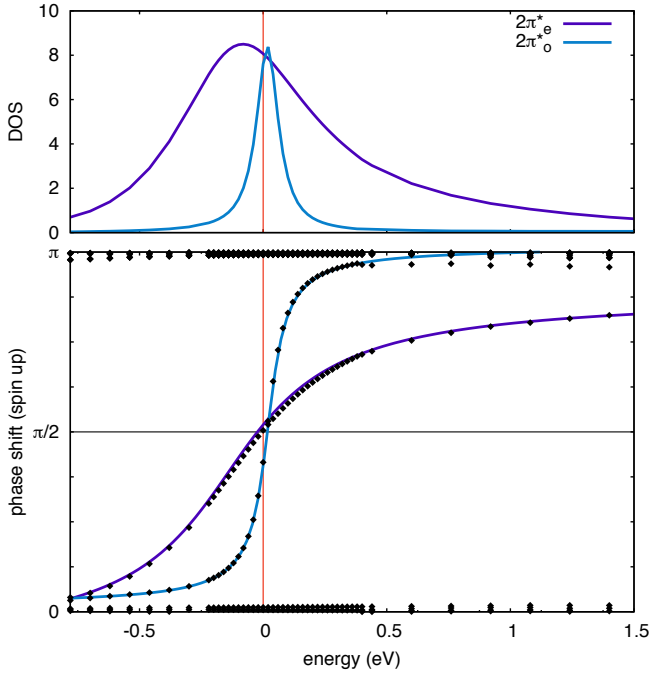
FIG. S2: Example of resonances in the scattering phase shifts and fits to Eq. S3.
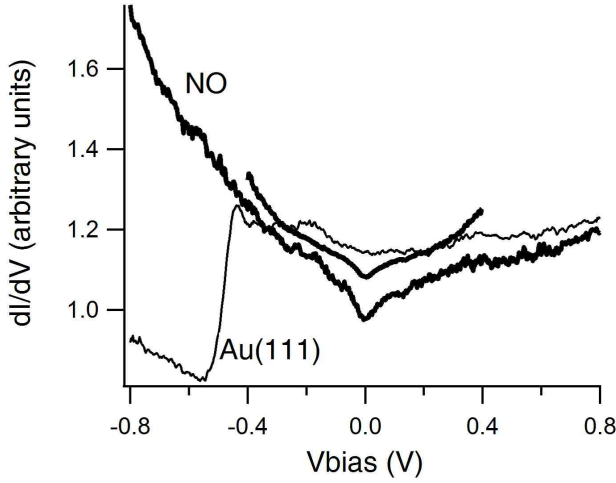

FIG. S3: STS spectra taken over NO molecules at 70 K (thick lines) and over the clean Au(111) surface a few nm away at 5 K (thin line).

TABLE S1: Ab initio properties of gas phase NO and NO/Au(111)

site	config.	E_{ads} (eV)	μ (μ_B)	d_{NO} (Å)	d_{AuN} (Å)	ν_{NO} (cm^{-1})	elec. dipole (D)
gas phase	—	—	1.00	1.1662	—	1885	0.109
				$(1.148)^a$		$(1903)^*$	$(0.157)^b$
on-top	tilted	0.320	0.89	1.1704	2.3309	—	0.353
bridge^c	vertical	0.148	0.94	1.1653	2.8206	—	0.313
fcc^c	vertical	0.122	1.14	1.1688	2.8576	—	0.172

^{a}Experiment, Ref. [2]
^{b}Experiment, Ref. [3]
^{c}Metastable configuration

TABLE S2: Anderson model parameters for NO/Au(111)

site	ϵ_e	ϵ_o	Γ_e	Γ_o	U_e	U_o	U_{eo}	J_H	W_{eo}
on-top	-0.92	-1.02	0.33	0.068	2.24	2.04	1.67	-0.807	-0.134
bridge	-1.22	-1.83	0.12	0.13	2.01	3.18	2.13	-0.807	-0.134
fcc	-1.00	-1.00	0.22	0.22	2.45	2.45	1.83	-1.06	-0.178

All quantities in eV; SDs of ϵ_e, ϵ_o, Γ_e and Γ_o for the on-top site are 0.04, 0.01, 0.036, and 0.015, respectively.